AGU100 ADVANCING EARTH AND SPACE SCIENCE

Geophysical Research Letters

RESEARCH LETTER
10.1029/2019GL085777

Diabatic Heating as a Pathway for Cyclone Clustering Encompassing the Extreme Storm Dagmar

C. Weijenborg[1] and T. Spengler[1]

[1]Geophysical Institute, University of Bergen, and Bjerknes Centre for Climate Research, Bergen, Norway

Abstract Contrary to the general notion that extratropical cyclones reduce baroclinicity, the baroclinicity is found to be enhanced in the wake of the extreme winter storm Dagmar. Thus, individual storms can increase baroclinicity, yielding a pathway to secondary cyclogenesis and cyclone clustering. We use a recently introduced diagnostic for baroclinicity—the tendency equation for the isentropic slope—and found that strong diabatic heating due to moisture supply from the subtropical Atlantic led to the enhanced baroclinicity in the rear of Dagmar. Storms ensuing Dagmar benefited from this increased baroclinicity. In contrast to previous studies on the mechanisms of cyclone clustering, we only find weak evidence for Rossby wave breaking and thus propose diabatic heating as an alternative pathway to cyclone clustering.

Key Points:
- Evolution of baroclinicity is investigated using the isentropic slope framework
- Isentropic framework is consistent with traditional energy framework without requiring a separation into mean and perturbation
- Diabatic heating associated with storm Dagmar yields an increased baroclinicity associated with cyclone clustering

Supporting Information:
- Supporting Information S1

Correspondence to:
C. Weijenborg,
christian.weijenborg@uib.no

Citation:
Weijenborg, C., & Spengler, T. (2020). Diabatic heating as a pathway for cyclone clustering encompassing the extreme storm Dagmar. *Geophysical Research Letters*, *47*, e2019GL085777. https://doi.org/10.1029/2019GL085777

Received 10 OCT 2019
Accepted 23 MAR 2020
Accepted article online 28 MAR 2020

1. Introduction

The extratropical cyclone Dagmar that developed over the North Atlantic around 24 December 2011 was one of the most extreme storms for western Norway (Martius et al., 2016; NVE, 2012). Such severe extratropical storms often occur in clusters with multiple intense cyclones succeeding each other in a short period of time (Mailier et al., 2006; McCallum & Norris, 1990; Pinto et al., 2014; Ulbrich et al., 2001). This was also the case in December 2011, when several strong cyclones reached the west coast of Norway in a week (Cusack, 2016). With the generally accepted paradigm of baroclinic instability for extratropical cyclones (Charney, 1947; Eady, 1949), one would anticipate that clustering coincides with increased baroclinicity, although simultaneously, the storms would be expected to reduce the baroclinicity. This apparent contradiction is investigated in this study, where we focus on how Dagmar influenced the baroclinicity and the ensuing cluster of cyclones.

Previous studies on clustering focus mainly on the spatiotemporal occurrence of cyclones in the Northern Hemisphere, finding that the exit region of the North-Atlantic jet is one of the main regions for cyclone clustering (Mailier et al., 2006; Vitolo et al., 2009). In this area, clustering of cyclones is often accompanied by an intensified eddy-driven jet that is zonally extended towards western Europe (Pinto et al., 2014; Priestley et al., 2017), kept in place by two-sided Rossby wave breaking (Barnes & Hartmann, 2012). These jet characteristics, however, do not explain why several storms occur in such a short period of time. Pinto et al. (2014) argues for the importance of secondary cyclogenesis as a mechanism for cyclone clustering, implying that significant baroclinicity is left behind preceding storms.

Similarly, the intensified jet during cyclone clustering (Priestley et al., 2017) suggests that there should be a temporary increase of baroclinicity due to thermal wind balance. This raises the question how baroclinicity increases despite the commonly accepted paradigm that individual cyclones should decrease baroclinicity during their life cycle. The climatological maintenance of storm tracks and baroclinicity (Hoskins & Valdes, 1990; Papritz & Spengler, 2015) implies that some cyclones have to significantly increase baroclinicity during their life cycle if the majority of cyclones reduces baroclinicity, which is consistent with baroclinicity not always being maintained on synoptic and weekly timescales (Novak et al., 2017; Thompson & Birner, 2012). Therefore, we hypothesize that individual cyclones can actually enhance baroclinicity throughout their life cycles.

To assess the evolution of the baroclinicity during the storm Dagmar and the ensuing clustering period, we employ the isentropic slope diagnostic of Papritz and Spengler (2015). While their study mainly focuses on the climatological analysis of the isentropic slope over the North Atlantic, the diagnostic also proves to be useful for the investigation of individual cyclones. One advantage compared with the Eady growth rate (Eady, 1949), which is almost identical to the isentropic slope, is that Papritz and Spengler (2015) derived

a diagnostic tendency equation for the isentropic slope. This tendency equation can be used to study both adiabatic and diabatic effects on the spatiotemporal evolution of baroclinicity.

Using the isentropic slope diagnostic, we investigate the life cycle of Dagmar with particular focus on the evolution of the baroclinicity over the North Atlantic storm track and the associated period of cyclone clustering. Given the importance of diabatic processes for more severe and faster growing cyclones (Fink et al., 2012; Reed et al., 1988; Schultz et al., 2019; Stoelinga, 1996; Tierney, 2018; Wernli et al., 2002), we also discuss the crucial role of moisture and associated latent heat release for this period. We complement our analysis with a comparison of the isentropic slope framework to the more traditional energy frameworks of Lorenz (1955) and Orlanski and Katzfey (1991) together with an overview of Rossby wave breaking during the event.

2. Methodology and Data

We use the ERA-Interim reanalysis from the European Centre for Medium Range Weather Forecasts (ECMWF)(Dee et al., 2011), which is available at a triangular truncation of T255 with a 6-hourly time interval providing analyses at 00, 06, 12, and 18 UTC. We interpolated the data onto a 0.5-degree grid and use the three-dimensional wind field, geopotential height z, temperature T, and diabatic heating $\dot{\theta}$ at 23 pressure levels (925, 900, 875, 850, 825, 800, 775, 750, 700, 650, 600, 550, 500, 450, 400, 350, 300, 250, 200, 150, and 100 hPa). The precipitation and the diabatic heating at the four analysis times were derived using the 6-hourly accumulated values around the respective time steps using the 00 and 12 UTC ERA-Interim forecasts (for details see supporting information).

As in Papritz and Spengler (2015), we define the isentropic slope S

$$S \equiv |\nabla_\theta z|, \tag{1}$$

with geopotential height z, where subscript θ indicates that the gradients are calculated along isentropic surfaces. The tendency equation for the isentropic slope is

$$\frac{DS}{Dt} = \frac{\nabla_\theta z}{S} \cdot \nabla_\theta w_{id} - \frac{\partial z}{\partial \theta} \frac{\nabla_\theta z}{S} \cdot \nabla_\theta \dot{\theta} + \mathbf{u} \cdot \nabla_\theta S, \tag{2}$$

with the isentropic displacement velocity $w_{id} = w - w_{iu}$, where w is the full vertical velocity and w_{iu} is referred to as isentropic upgliding (Hoskins et al., 2003). We refer to the three terms on the right hand side as the tilting, diabatic, and flux term, respectively.

The physical interpretation of the tilting term is the classical rearrangement of mass during baroclinic instability (Papritz & Spengler, 2015). For a growing midlatitude cyclone, warm air ascends poleward, while cold air descends equatorward. The net effect is that the isentropes are flattened. Alternatively, this process describes the conversion from available potential energy to kinetic energy (Lorenz, 1955). The second term is associated with the modification of the isentropic slope due to diabatic heating. In extratropical cyclones, the latter is mainly associated with surface fluxes in the lower and latent heating in the middle troposphere, where both processes lead to a local increase of the isentropic slope (Papritz & Spengler, 2015). Diabatic heating yields a secondary circulation that indirectly influences w_{id}. Similar to the Lorenz (1955) energy framework, there is, however, no direct impact of the heating on the tilting term. The third term is associated with the movement of fronts and is generally smaller than the other two terms.

We averaged the diagnostics for the isentropic slope vertically over the troposphere from 900 to 200 hPa. As the isentropic slope is inversely proportional to the static stability, we set grid points with a vertical gradient $\frac{d\theta}{dz}$ below a threshold of 0.5 K km^{-1} as undefined.

As the isentropic slope diagnostic has thus far not been compared to the energy framework of Lorenz (1955) and Orlanski and Katzfey (1991), we provide such a synoptic analysis where we applied a time mean of 30 days centered around the event (11 December 2011 to 10 January 2012) to distinguish between mean and eddy quantities (for details see supporting information). Furthermore, we complement the isentropic slope analysis with both an instantaneous blocking index (Masato et al., 2013) and a Rossby wave breaking index that distinguishes between anticyclonic and cyclonic wave breaking (Rivière, 2009).

3. Synoptic Evolution Around the Storm Dagmar

Dagmar formed on 23 December 2011 but mainly intensified after 24 December 0 UTC over the eastern Atlantic. At that time, a strong jet is present over the western Atlantic with maximum wind speed up to 70

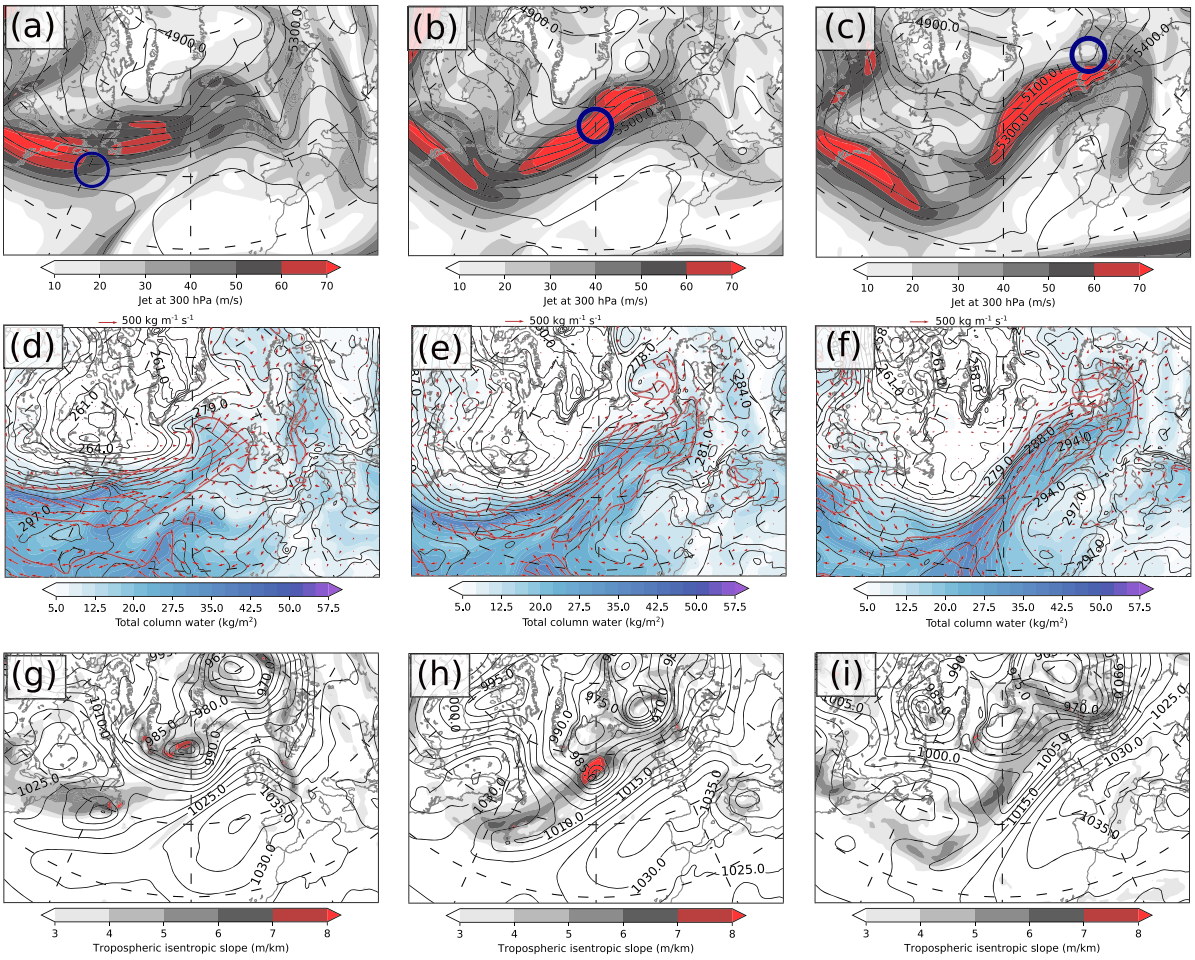

Figure 1. Synoptic evolution for Dagmar (blue circle) with the left panels for 24 December 2011 0 UTC (formation of Dagmar), middle panels for 25 December 0 UTC (maximum intensification of Dagmar), and right panels for 26 December 0 UTC (decay of Dagmar). (a–c) Atmospheric jet at 300 hPa (shading, in m s^{-1}) and geopotential height at 500 hPa (contours, in m). (d–f) Vertically integrated water vapor (shading, in kg m^{-2}), moisture flux (red arrows, red contour line indicates a moisture flux above 250 kg m^{-1} s^{-1}), and θ at 850 hPa (contours, every 3 K). (g–i) Isentropic slope (shading, in m km^{-1}) and the mean sea level pressure (contours, in hPa).

ms^{-1}, whereas the jet over the eastern Atlantic is still weak and unorganized (Figure 1a). Consistently, the baroclinicity is also mainly limited to the western part of the Atlantic (Figure 1g). The strongest isentropic slopes are found near the core of the cyclone at the region of the bent-back front (Figure 1g), which is consistent with the discussion of Papritz and Spengler (2015). The atmospheric water content features a strong gradient in the western Atlantic, separating dry subpolar from rather moist subtropical air masses (Figure 1d), whereas the eastern Atlantic appears relatively well mixed latitudinally.

During the next 24 hours, Dagmar intensified rapidly with a drop from 994 to 956 hPa, classifying the storm as a bomb cyclone (Sanders & Gyakum, 1980). Simultaneously, the jet intensified and extended eastward across the Atlantic (Figure 1b), which is also visible as enhanced baroclinicity in the wake of Dagmar (Figure 1h). The westward tilt between mean sea level pressure (Figure 1h) and geopotential height at 500 hPa (Figure 1e) was favorable for the intensification of Dagmar. Another important contribution to the rapid development of Dagmar is associated with the ample supply of moisture that spurred the diabatic intensification (Figure 1e). Dagmar featured strong fronts at this time and especially the cold front intensified further during the next 12 hours (not shown).

On 26 December 0 UTC, Dagmar reached Western Norway and started to decay (Figure 1i), which highlights the rapid evolution and movement of the storm crossing the entire Atlantic in less than 2 days. At this time, the jet extended further into Western Norway (Figure 1c), still featuring moderately strong baroclinicity over the entire Atlantic (Figure 1i). Only a weak disturbance is visible over the mid-Atlantic at this

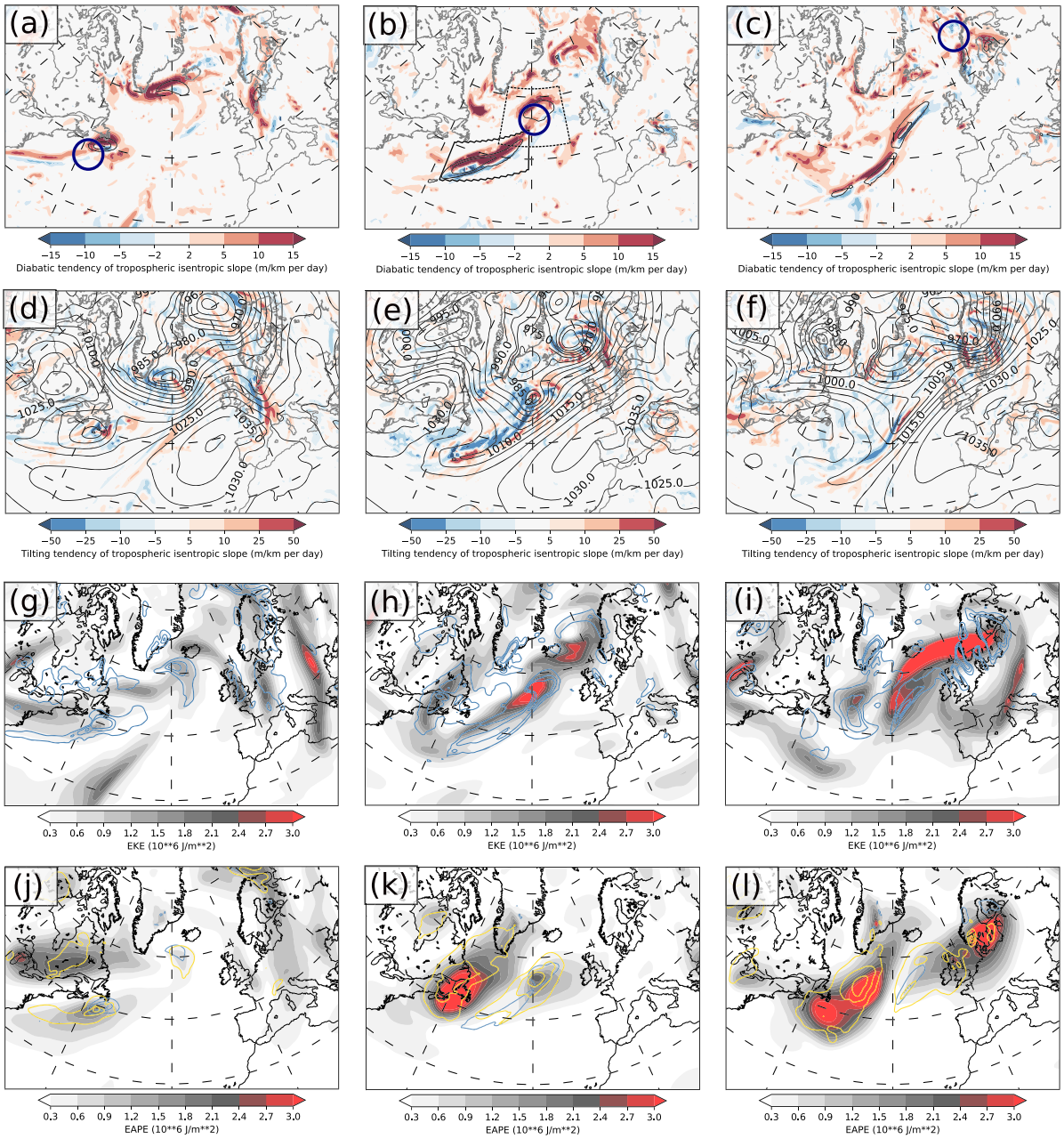

Figure 2. Tendencies of the isentropic slope and energy analysis for Dagmar (blue circle) with the left panels for 24 December 2011 0 UTC (formation of Dagmar), middle panels for 25 December 0 UTC (maximum intensification of Dagmar), and right panels for 26 December 0 UTC (decay of Dagmar). (a–c) Diabatic tendencies (shading, in m km^{-1} per day) and total precipitation (contours, with 1, 2 m mh^{-1}). Dashed and solid boxes in (b) indicate the areas for the slope budget around Dagmar and along the cold front, respectively. (d–f) Tilting tendencies (shading, in m km^{-1} per day) and the mean sea level pressure (contours, in hPa). (g–i) Eddy kinetic energy (shading, in 10^6 J m^{-2}) and conversion from eddy available potential energy to eddy kinetic energy (blue contours, at 20, 60, 100 W m^{-2}). (j–l) Eddy available potential energy (shading, in 10^6 J m^{-2}) and the baroclinic (gold contours, at 20, 60, 100 W m^{-2}) and diabatic generation (blue contours, at 20, 60, 100 W m^{-2}) of eddy available potential energy.

time (Figures 1i and S1), but several cyclones formed in the west Atlantic about 2 days later leading to the associated period of cyclone clustering.

The moisture plume in Figures 1e and 1f across the North Atlantic satisfies the definition of an atmospheric river (e.g., Rutz et al., 2014), with significant amounts of moisture reaching the west coast of Norway that led to heavy precipitation in association with orographic lift (Martius et al., 2016). The significant moisture flux

convergence along the cold front (not shown) is argued to be responsible for the band of high total column water vapor associated with the atmospheric river (Dacre et al., 2015).

4. Build-up of Baroclinicity Across the North Atlantic

On 24 December 0 UTC, the diabatic forcing of the tropospheric isentropic slope near the core of Dagmar is clearly discernible (Figure 2a). This signature intensifies 1 day later, where also an elongated trail of diabatic forcing is visible in the western Atlantic (Figure 2b), which is aligned with the strong moisture gradient (Figure 1e). The diabatic intensification just downstream of the core of Dagmar was most likely beneficial for the rapid cyclone development, because the eastward moving cyclone can directly consume the enhanced baroclinicity. The strong diabatic tendencies along the trailing cold front, on the other hand, contributed to the formation of the intense baroclinicity in the wake of Dagmar. The diabatic tendencies at the trailing cold front are mainly attributable to latent heat release associated with large-scale and convective precipitation (Papritz & Spengler, 2015). This diabatic intensification is the main contributor to the enhanced baroclinicity trailing Dagmar (Figure 1g). On 26 December 0 UTC, there is still a diabatic signature in the tendency of the isentropic slope across most of the central Atlantic in alignment with the strong gradient in moisture (Figure 1f) and just south of the jet (Figure 1c).

The tilting tendencies are relatively weak on 24 December 0 UTC (Figure 2d) but rose to rather intense levels one day later (Figure 2e), with strongly negative tilting tendencies around Dagmar (-5.80 m km^{-1} per day averaged over box defined in Figure 2b). The negative average tilting tendencies are consistent with the baroclinic intensification of cyclones (Papritz & Spengler, 2015). The bands of positive and negative values in the tilting tendency arise due to the isentropic displacement velocity in equation (**?**) also accounting for the movement of fronts. In conjunction with the onsetting decay of the storm Dagmar, the tilting is diminished 26 December 0 UTC (Figure 2f).

Comparing the evolution of the baroclinicity along the trailing cold front (Figures 1g– 1i), the positive diabatic forcing outweighed the negative tilting forcing (Figures 2a–2f), leading to the formation of the enhanced baroclinicity in the wake of Dagmar that presumably contributed to the formation of the ensuing cluster of storms (see section 6). However, with the diabatic heating accumulated over 6 hr and instantaneous fields used for the two kinematic tendencies, the latter are generally overestimated (4.61 m km^{-1} per day compared to -4.83 m km^{-1} per day, averaging box defined in Figure 2b), which renders a quantitative comparison difficult.

5. Energetics of the Evolution

Complementing the above results with the energy framework of Lorenz (1955) and Orlanski and Katzfey (1991), we find that the eddy kinetic energy features a strong increase over the central Atlantic within 24 hr between 24 and 25 December (Figures 2g and 2h). This is associated with the intensification of Dagmar coinciding with the conversion of eddy available energy towards eddy kinetic energy (Figure 2h) and is consistent with the tilting tendency of the isentropic slope (Figure 2e). During the next 24 hr, the evolution of the eddy kinetic energy appears to be mainly associated with the intensification of the jet (Figures 1c and 2i). The conversion to eddy kinetic energy, however, still largely aligns with the tilting tendency of the isentropes, with centres of action above northern Scandinavia and the central Atlantic (Figures 2f and 2i).

The maxima in eddy available potential energy on 24 December over the western and central Atlantic (Figure 2j) demarcate the development of Dagmar. These two features progress eastward across the Atlantic the next 2 days, while the eddy available potential energy that resided over the eastern United States moves over the western Atlantic and intensifies (Figures 2k and 2l). This feature in eddy available potential energy is not visible in the isentropic slope due to the stability threshold (Figures 1h and 1i) and classifies as a cold air outbreak over the northeastern Atlantic (Papritz et al., 2015). A larger scale temperature anomaly is not necessarily associated with sloping isentropes, although there are some hints of the cold air outbreak in the lower level isentropic slope (Figure S1b).

The increase of eddy available potential energy in Dagmar and the ensuing cyclone have a large contribution from diabatic generation of eddy available potential energy (Figure 2k). There is a significant overlap

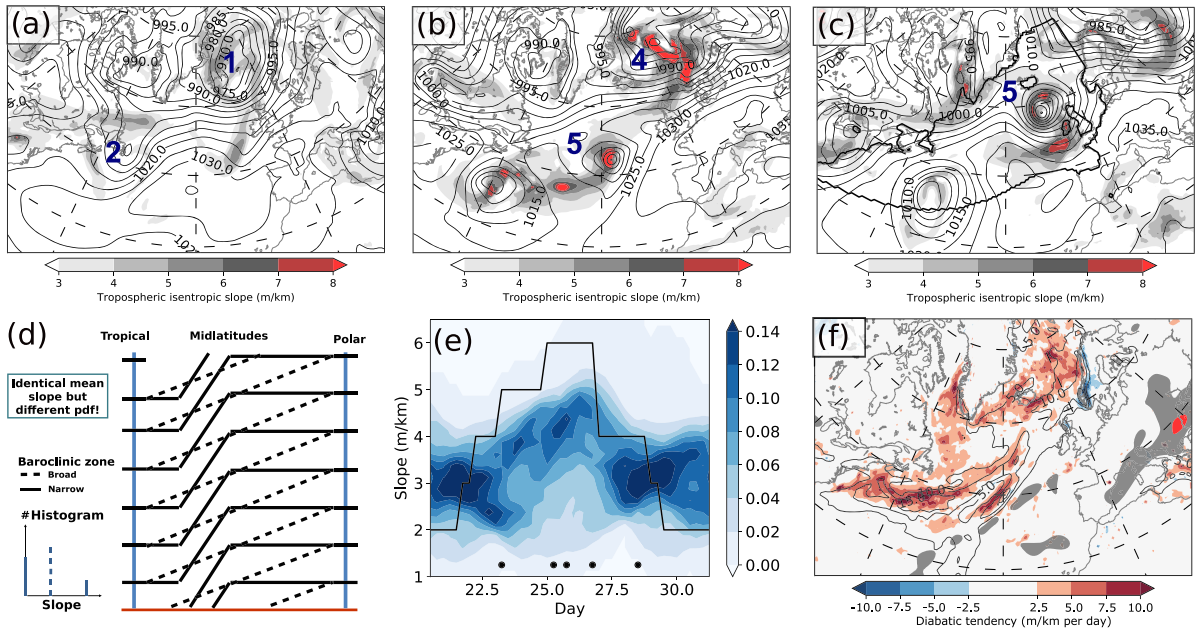

Figure 3. (a–c) Isentropic slope (shading, in m km^{-1}) and the mean sea level pressure (contours, in hPa) for 23 December 00 UTC (left panel), 27 December 00 UTC (middle panel), and 28 December 00 UTC (right panel). The sequence of storms in the cluster is indicated by numbers. (d) Schematic of isentropic slopes for a broad baroclinic zone (dashed lines) and a narrow baroclinic zone (solid lines). Both situations have an identical mean slope but a different distribution, which is indicated in the histogram in the lower left corner. (e) Normalized histogram of baroclinicity from 20 to 30 December 2011 (calculated over region where seasonal mean slope is above 2.5 m km^{-1}, indicated by the black contour line in c). Black line indicates running mean of number of storms reaching the East Atlantic (indicated by dots). (f) Average diabatic tendency (shading, in m km^{-1} per day) and precipitation (contour lines, every 5 mm per day), and percentage of time steps with Rossby wave breaking according to Rivière (2009) (gray and red shadings indicate 10% and 20% levels, respectively) from 23 December 12 UTC until 28 December 12 UTC.

of diabatic generation of eddy available potential energy and the conversion towards eddy kinetic energy (Figures 2h and 2k), suggesting a direct diabatic intensification of the storm. The diabatic generation of eddy available potential energy (Figures 2j– 2l) can also be directly related to the diabatic generation of isentropic slope (Figures 2a– 2c).

There is also a significant contribution due to baroclinic conversion to eddy available potential energy, especially within the cold air mass, which is not visible in the diagnostics for the isentropic slope. This is partially due to the stability threshold, which focuses the isentropic slope diagnostic more on the large-scale baroclinic development without emphasizing the development of the surface-based cold air outbreak. The emphasis of the temperature anomaly in the traditional energy framework is also largely associated with the separation of the flow in eddy and mean components. The isentropic slope diagnostic, on the other hand, does not suffer from such an a priori separation.

6. Cyclone Clustering

Several cyclones crossed the Atlantic in a short period of time prior and subsequent to Dagmar. In fact, Dagmar resulted from a secondary cyclogenesis along the cold front of the preceding extreme storm named Cato (Figures 1d and 1g). In conjunction with the clustering of these cyclones, the jet intensified from 23 December and remained very zonal and intense (Figures 1a– 1c) until 27 December. Before and after this period, the jet was rather unstructured (Figures S3a and S3c). Pinto et al. (2014) argued that the intense jet during cyclone clustering is associated with two-sided Rossby wave breaking. Weak Rossby wave breaking for this case, however, is only detected south of the jet (Figure S4), which is consistent with Priestley et al. (2017), who found that clustering at higher latitudes (65°N) is mainly accompanied by Rossby wave breaking south of the jet. Some reversal of the meridional geopotential height gradient can be detected on the northern side when using the algorithm of Masato et al. (2013) (Figure S4), although this is probably not associated with Rossby wave breaking (Spensberger et al., 2017).

The evolution of the jet is mirrored by the evolution of the baroclinicity (Figures 1g– 1i and 3a–3c). A narrowing of the baroclinic zone does not necessarily lead to an increase of the mean isentropic slope

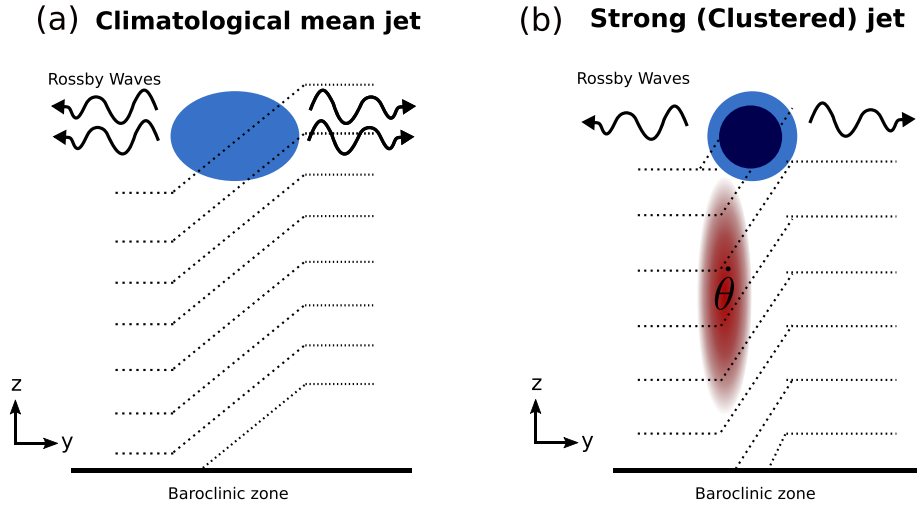

Figure 4. Schematic of jet (blue solid circle), isentropic slope (dashed contour lines indicate isentropes), and Rossby waves (wavy arrows). (a) Climatologically, there is a broad baroclinic zone and relatively weak jet. (b) During clustering there is excessive heating at the southern side of the jet leading to increased baroclinicity and an intense jet.

over the Atlantic, as the mean slope is solely determined by the position of the isentropic surfaces along the lateral boundaries. For example, given the same mean isentropic slope over a certain domain, the distribution of the isentropic slope for a broad baroclinic zone would feature a median value close to the mean (dashed line in Figure 3d), whereas the distribution of the isentropic slope for a narrow baroclinic zone would be characterized by a distribution featuring both extreme values as well as rather low values (solid line in Figure 3d).

The normalized 5-day low-pass filtered isentropic slope over the Atlantic shows that the increase of higher slope values coincides with the intensification of Dagmar (Figure 3e). Thus, the clustering period with a total of five storms reaching the East Atlantic within 5 days (dots at bottom of Figure 3e) coincided with enhanced isentropic slopes. The first two storms already featured minimum sea level pressures below 960 hPa, with Dagmar being the third and strongest storm in the cluster, followed by two consecutive storms (Figure 3). The accumulated diabatic slope tendency across the Atlantic agrees well with the area of increased baroclinicity and storm formation, whereas Rossby wave breaking mainly occurs over central and southern Europe (Figure 3f). The breakup of the enhanced baroclinicity after 27 December (Figures 3b and 3c, see Figure S5 for the tendencies) is associated with the cyclone developing in the eastern Atlantic at that time. In contrast to the preceding cyclones, this cyclone featured a significant frontal wrap-up in conjunction with a cold air outbreak on its western flank that suppressed the moisture supply and split the jet stream (Figures 3b and S3). The split of the jet possibly also reduced the propagation of the cyclone, leading to the more efficient frontal wrap-up.

Rossby wave breaking has been argued to be important for intensifying the jet (Pinto et al., 2014; Priestley et al., 2017), although diabatic heating can also play a crucial role in strengthening the baroclinicity and the jet. In the transformed Eulerian mean (TEM), neglecting external forces like friction, the evolution of the zonal mean zonal wind $\bar{u}$ is given by (e.g., Vallis, 2017)

$$\frac{\partial \bar{u}}{\partial t} = \overline{v'q'} + f_0 \bar{v}^*, \tag{3}$$

where $\bar{u}$ is the zonal mean zonal wind velocity, $\overline{v'q'}$ is the meridional potential vorticity flux, and $\bar{v}^*$ is the residual meridional flow. The first term on the right-hand side is equivalent to the divergence of the Eliassen-Palm flux, which is associated with Rossby wave propagation that maintains the climatological jet (e.g., Barnes & Hartmann, 2012; Vallis, 2017, see Figure 4a).

We applied equation (3) to quantify the relative contributions of Rossby wave breaking and diabatic heating to the jet intensification. The TEM framework did, however, not provide a conclusive answer (Figure S6), which is most likely due to its dependence on the choice of a zonal mean and the difficulties incorporating suitable boundary conditions. On the other hand, the isentropic slope framework diagnoses a significant

diabatic intensification of baroclinicity, which, through thermal wind, implies an intensification of the jet. This supports the alternative hypothesis that diabatic heating along the southern flank of the baroclinic zone enhanced the baroclinicity, thereby intensifying the jet, which provides a conducive environment for cyclone clustering (Figure 4b).

7. Discussion and Concluding Remarks

We diagnosed a cyclone clustering period associated with the extreme storm Dagmar using the isentropic slope framework that provides a tendency equation for the kinematic and diabatic contributions to changes in baroclinicity (Papritz & Spengler, 2015). We showed that the isentropic slope diagnostic is an adequate tool to diagnose individual cyclone development and that the framework is consistent with the traditional energy analysis (Lorenz, 1955; Orlanski & Katzfey, 1991), with the advantage that it does not depend on the separation into an eddy and mean state.

Contrary to the generally accepted notion that baroclinic instability reduces baroclinicity, we find that individual cyclones can enhance the baroclinicity on scales larger than the storm itself. The increase of baroclinicity in the wake of Dagmar was due to intense diabatic heating associated with the exhaustive availability of moisture along an atmospheric river stretching across the North Atlantic. Thus, storms do not only convert baroclinicity into growth, but they also replenish baroclinicity through diabatic heating. This is consistent with the concept of climatological self-maintenance of storm tracks (Hoskins & Valdes, 1990; Papritz & Spengler, 2015), although the Dagmar case demonstrates that an individual storm can actually yield a net increase in baroclinicity on synoptic timescales.

The phases of growth and decay of the large-scale baroclinicity for Dagmar are rather fast, and it only takes less than a week to develop and then destroy the sharp baroclinic zone. The clustering of five cyclones during this time period concurs with this temporary increase of baroclinicity. Such short-term variations of baroclinicity are consistent with the pulsating nature of storm track activity (Novak et al., 2017, 2018; Thompson & Birner, 2012, 2014), although these variations occur on longer timescales compared to the rapid buildup and decay presented here.

Based on our findings, we propose the increase of baroclinicity through diabatic heating as a pathway to cyclone clustering. This process could work in isolation or in conjunction with the previously proposed contribution of Rossby wave breaking (Pinto et al., 2014; Priestley et al., 2017). Further analysis has to quantify the respective diabatic and kinematic contributions that strengthen the baroclinicity and the jet during periods of cyclone clustering.

Acknowledgments
This study was supported by UNPACC (NFR Project 262220). The authors are grateful to ECMWF for providing the ERA-Interim reanalyses for free at https://apps.ecmwf.int/datasets/data/interim-full-daily/levtype=pl/. The authors thank the 2 anonymous reviewers for their comments which helped improving the quality of the manuscript.

References

Barnes, E. A., & Hartmann, D. L. (2012). Detection of Rossby wave breaking and its response to shifts of the midlatitude jet with climate change. *Journal of Geophysical Research*, *117*, D09117. https://doi.org/10.1029/2012JD017469

Charney, J. G. (1947). The dynamics of long waves in a baroclinic westerly current. *Journal of Meteorology*, *4*(5), 136–162.

Cusack, S. (2016). The observed clustering of damaging extratropical cyclones in Europe. *Natural Hazards and Earth System Sciences*, *16*(4), 901–913. https://doi.org/10.5194/nhess-16-901-2016

Dacre, H. F., Clark, P. A., Martinez-Alvarado, O., Stringer, M. A., & Lavers, D. A. (2015). How do atmospheric rivers form? *Bulletin of the American Meteorological Society*, *96*(8), 1243–1255.

Dee, D. P., Uppala, S., Simmons, A., Berrisford, P., Poli, P., Kobayashi, S., et al. (2011). The ERA-Interim reanalysis: Configuration and performance of the data assimilation system. *Quarterly Journal of the Royal Meteorological Society*, *137*(656), 553–597.

Eady, E. T. (1949). Long waves and cyclone waves. *Tellus*, *1*(3), 33–52.

Fink, A. H., Pohle, S., Pinto, J. G., & Knippertz, P. (2012). Diagnosing the influence of diabatic processes on the explosive deepening of extratropical cyclones. *Geophysical Research Letters*, *39*, L07803. https://doi.org/10.1029/2012GL051025

Hoskins, B. J., Pedder, M., & Jones, D. W. (2003). The omega equation and potential vorticity. *Quarterly Journal of the Royal Meteorological Society*, *129*(595 PART B), 3277–3303. https://doi.org/10.1256/qj.02.135

Hoskins, B. J., & Valdes, P. J. (1990). On the existence of storm-tracks. *Journal of the Atmospheric Sciences*, *47*(15), 1854–1864.

Lorenz, E. N. (1955). Available potential energy and the maintenance of the general circulation. *Tellus*, *7*(2), 157–167. https://doi.org/10.3402/tellusa.v7i2.8796

Mailier, P. J., Stephenson, D. B., Ferro, C. A., & Hodges, K. I. (2006). Serial clustering of extratropical cyclones. *Monthly Weather Review*, *134*(8), 2224–2240.

Martius, O., Pfahl, S., & Chevalier, C. (2016). A global quantification of compound precipitation and wind extremes. *Geophysical Research Letters*, *43*, 7709–7717. https://doi.org/10.1002/2016GL070017

Masato, G., Hoskins, B. J., & Woollings, T. (2013). Wave-breaking characteristics of northern hemisphere winter blocking: A two-dimensional approach. *Journal of Climate*, *26*(13), 4535–4549.

McCallum, E., & Norris, W. J. T. (1990). The storms of January and February 1990. *Meteorological Magazine*, *119*, 201–210.

NVE (2012). Vinden som blåste i fjor. Hvor sterk var Dagmar? (Vol. 42; Tech. Rep.). Norges vassdrags- og energidirektorat.

Novak, L., Ambaum, M. H. P., & Harvey, B. J. (2018). Baroclinic adjustment and dissipative control of storm tracks. *Journal of the Atmospheric Sciences*, *75*, 2955–2970. https://doi.org/10.1175/JAS-D-17-0210.1

Novak, L., Ambaum, M. H. P., & Tailleux, R. (2017). Marginal stability and predator prey behaviour within storm tracks. *Quarterly Journal of the Royal Meteorological Society*, *143*(704), 1421–1433. https://doi.org/10.1002/qj.3014

Orlanski, I., & Katzfey, J. (1991). The life cycle of a cyclone wave in the Southern Hemisphere. Part I: Eddy energy budget. *Journal of Atmospheric Sciences*, *48*, 1972–1998. https://doi.org/10.1175/1520-0469(1991)048<1972:TLCOAC>2.0.CO;2

Papritz, L., Pfahl, S., Sodemann, H., & Wernli, H. (2015). A climatology of cold air outbreaks and their impact on air–sea heat fluxes in the high-latitude south pacific. *Journal of Climate*, *28*(1), 342–364.

Papritz, L., & Spengler, T. (2015). Analysis of the slope of isentropic surfaces and its tendencies over the North Atlantic. *Quarterly Journal of the Royal Meteorological Society*, *141*(693), 3226–3238. https://doi.org/10.1002/qj.2605

Pinto, J. G., Gómara, I., Masato, G., Dacre, H. F., Woollings, T., & Caballero, R. (2014). Large-scale dynamics associated with clustering of extratropical cyclones affecting Western Europe. *Journal Geophysical Research: Atmospheres*, *119*, 13,704–13,719. https://doi.org/10.1002/2014JD022305

Priestley, M. D. K., Pinto, J. G., Dacre, H. F., & Shaffrey, L. C. (2017). Rossby wave breaking, the upper level jet, and serial clustering of extratropical cyclones in western Europe. *Geophysical Research Letters*, *44*, 514–521. https://doi.org/10.1002/2016GL071277

Reed, R. J., Albright, M. D., Sammons, A. J., & Undén, P. (1988). The role of latent heat release in explosive cyclogenesis: Three examples based on ecmwf operational forecasts. *Weather and Forecasting*, *3*(3), 217–229.

Rivière, G. (2009). Effect of latitudinal variations in low-level baroclinicity on eddy life cycles and upper-tropospheric wave-breaking processes. *Journal of the Atmospheric Sciences*, *66*(6), 1569–1592.

Rutz, J. J., Steenburgh, W. J., & Ralph, FMartin (2014). Climatological characteristics of atmospheric rivers and their inland penetration over the western united states. *Monthly Weather Review*, *142*(2), 905–921.

Sanders, F., & Gyakum, J. R. (1980). Synoptic-dynamic climatology of the "bomb". *Monthly Weather Review*, *108*(10), 1589–1606.

Schultz, D. M., Bosart, L. F., Colle, B. A., Davies, H. C., Dearden, C., Keyser, D., et al. (2019). Extratropical cyclones: A century of research on meteorology's centerpiece. *Meteorological Monographs*, *59*, 16.1–16.56. https://doi.org/10.1175/amsmonographs-d-18-0015.1

Spensberger, C., Spengler, T., & Li, C. (2017). Upper-tropospheric jet axis detection and application to the boreal winter 2013/14. *Monthly Weather Review*, *145*(6), 2363–2374. https://doi.org/10.1175/mwr-d-16-0467.1

Stoelinga, M. T. (1996). A potential vorticity-based study of the role of diabatic heating and friction in a numerically simulated baroclinic cyclone. *Monthly Weather Review*, *124*(5), 849–874.

Thompson, D. W. J., & Barnes, E. A. (2014). Periodic variability in the large-scale Southern Hemisphere atmospheric circulation. *Science*, *343*(6171), 641–645. https://doi.org/10.1126/science.1247660

Thompson, D. W. J., & Birner, T. (2012). On the linkages between the tropospheric isentropic slope and eddy fluxes of heat during Northern Hemisphere winter. *Journal of the Atmospheric Sciences*, *69*(6), 1811–1823. https://doi.org/10.1175/jas-d-11-0187.1

Tierney, G. (2018). An examination of extratropical cyclone response to changes in baroclinicity and temperature in an idealized environment. *Climate Dynamics*, *51*, 3829–3846. https://doi.org/10.1007/s00382-018-4115-5

Ulbrich, U., Fink, A., Klawa, M., & Pinto, J. G. (2001). Three extreme storms over Europe in December 1999. *Weather*, *56*(3), 70–80.

Vallis, G. K. (2017). *Atmospheric and oceanic fluid dynamics*. Cambridge: Cambridge University Press.

Vitolo, R., Stephenson, D. B., Cook, I. M., & Mitchell-Wallace, K. (2009). Serial clustering of intense European storms. *Meteorologische Zeitschrift*, *18*(4), 411–424.

Wernli, H., Dirren, S., Liniger, M. A., & Zillig, M. (2002). Dynamical aspects of the life cycle of the winter storm 'Lothar' (24-26 December 1999). *Quarterly Journal of the Royal Meteorologial Society*, *128*(580), 405–429.